Composites Part C: Open Access 4 (2021) 100079

Contents lists available at ScienceDirect

Composites Part C: Open Access

journal homepage: www.elsevier.com/locate/jcomc

Experimental and numerical investigation on the impact response of CFRP under 3-point-bending

M. Nebe[a,*], T. Schmack[a,b], T. Schaefer[c], F. Walther[a]

[a] Department of Materials Test Engineering (WPT), TU Dortmund University, Baroper Str. 303, 44227 Dortmund, Germany
[b] Lightweight Center, Audi AG, NSU-Straße 1, 74148 Neckarsulm, Germany
[c] Department of Lightweight Technology (LBT), Karlsruhe Institute of Technology (KIT), Rintheimer-Querallee 2, 76131 Karlsruhe, Germany

ARTICLE INFO

Keywords:
Carbon fiber
Epoxy
Prepreg
Strain rate
Component testing
3-Point-bending
Finite element analysis

ABSTRACT

The strain rate-dependent material characteristic of carbon fiber reinforced plastics (CFRP) is widely known and has been investigated in detail at coupon level. In this study, for the first time the strain rate dependent characteristic of a three-dimensional CFRP structure was investigated. The evolution of the determined strain rate dependency was correlated with the results at coupon level. For this purpose two special 3-point-bending fixtures were developed to obtain the flexural impact response of the investigated T700S DT120 prepreg system at coupon and component (hat profile) level. The rectangular coupon specimens were loaded with quasi-static to intermediate impact velocities from 3.3×10^{-5} to 10m $s^{-}1$, while the structural sub components were tested using impact velocities from 3.3×10^{-5} to 1m $s^{-}1$. With increasing impact velocities, the experimental tests showed a significant increase in force at first failure and maximum deflection at coupon level. The increases in force were of 52% and 120%, respectively. However, the increase for structural hat profile components was just 12.4% due to a different failure mode. The observed initial failure modes were compressive failure provoked by fiber kinking for the coupon and interlaminar shear failure for the structural component. Regardless of the different failure modes this work proves the necessity of considering the strain rate dependency of a composite material to accurately predict the maximum load capacity of a CFRP structure during a dynamic load event. Additionally, the comparison of the experimental results restults to numerical results revealed weaknesses in the prediction accuracy of the currently used models.

1. Introduction

Although carbon fiber reinforced plastics (CFRP) can be found in sport car bodies, the usage in high volume automotive body structures is still a rarity. The main goal in body structure development is to design lightweight and stiff structures as cost-efficient as possible. A major key component in pricing is the elevated cost of carbon fiber. To close the gap to conventional metal structures, the full potential of CFRP has to be exploited in the design process. This research contributes to the approach of maximal material usage for relevant crash applications by considering the strength increase of CFRP with increasing strain rate.

The research boundaries in terms of numerical approaches are highly connected to the requirements of full vehicle crash simulations in the automotive environment. Major requirement and limitation is the usage of shell elements to save computational effort of the huge models (≈ 10 million elements). One of the element's type major restrictions is the missing ability to consider delaminations. Knowing this restrictions and challenges there is a need to perform multiple validation steps to obtain reliable predictions of the results obtained from simulations and experiments. For this purpose a kind of building block approach, subjecting different geometrical shapes of the specimen/ structure to different dynamical loading scenarios, is required. These dynamic tests are highly challenging in terms of force and strain measurements, signal processing and data analysis. Hence, this study presents two specially developed fixtures to load coupons and structural components by quasi-static and dynamic 3-point-bending. The obtained force-displacement curves are analysed by their change in strength with increasing strain rate and compared to the equivalent properties obtained from numerical simulation.

During a crash event, body structures are subjected to dynamical flexural loadings. This results in multi-axial stress states in which the strain rate-dependent response needs to be investigated. As stated in previous multiscale investigations [1,2] it is possible to transfer the results of strain rate dependency from coupon to structural component level. This has been proven for an axial compression load case scenario – experimentally and numerically.

* Corresponding author.
E-mail address: martin.nebe@tu-dortmund.de (M. Nebe).

https://doi.org/10.1016/j.jcomc.2020.100079
Received 7 August 2020; Accepted 25 November 2020

At coupon level, a well-known strain rate dependency of CFRP is stated in literature. The investigations reported strain rate effects on the mechanical properties of carbon epoxy laminates such as: shear [3,4], transverse [5,6] and longitudinal compression [7–9], and transverse in tension [10,11]. One of the first studies in the field of dynamical 3-point-bending on carbon epoxy laminates was performed by Lifshitz et al. [12]. Using a drop tower AS4/3502 carbon epoxy specimens were subjected to dynamical flexural loading. The resulting forces were derived by pre-processing the signal of an acceleration sensor multiplying with the impactors mass. Comparable investigations were carried out by Sánchez-Sáez et al. [13] using a drop tower equipped with a force sensor. Both studies report no significant increase in maximum force at first failure for all tested laminates. A plausible explanation is found in the initial failure type by reaching the longitudinal tensile strength on the bottom side of all specimens. Multiple studies investigating the longitudinal tensile properties of carbon epoxy laminates reported no change of the mechanical properties with increasing strain rate [10,11,14]. $[0°/90°]_{3s}$ and $[90°/0°]_{3s}$ carbon epoxy laminates were tested in a 3-point-bending by Wiegand [15], where 0°-direction is in accordance with the longitudinal beam axis. The quasi-static experiments were carried out using a universal screw driven testing machine. The dynamical tests utilized an impactor accelerated by a gas gun. The test set-up functional principle was identical to a method used by Hallett [16]. The fixture was used in different configurations, the support span was varied in two distances (30mm and 50mm) resulting in a short and long beam configuration. The $[0°/90°]_{3s}$ specimens showed for the dynamical loading compared to the quasi-static test an increase in maximal force at first failure and fracture strain of approx 54% and 58%, respectively. All specimens failed by reaching the ultimate compressive strength at the top side of the specimen characteristically by fiber kinking. For the $[0°/90°]_{3s}$ specimens, at 30mm support span a first failure was initiated by reaching the compressive strength of the matrix at the really top layer of the specimen or by fiber kinking of the second layer seen from the top. The dynamical maximum force at first failure was approx 30% (30mm support span) to 80% (50mm support span) higher compared to the quasi-static loading. The 50mm support span in combination with the $[0°/90°]_{3s}$ specimens resulted in fiber kinking as well as fiber tensile failure. Additionally, all dynamical tests in this configuration showed fiber tensile failure as initial failure type. In accordance with the studies from Lifshitz et al. [12] and Sánchez-Sáez et al. [13] no significant influence of the loading rate on the maximal force or ultimate strain was observed when fiber tensile failure occurs. Carpentier [17] performed 3-point-bending tests using a short beam configuration to obtain the shear properties of the tested carbon epoxy laminate. The shear strain γ_{13} and the initial failure mode of interlaminar shear failure was determined by using high-speed DIC system. For the dynamic tests at 4.4m s^{-1} impact velocity ($\dot{\varepsilon} \approx 100s^{-1}$), an increase in maximum force was found. The shear strength and shear modulus from the dynamical tests compared to the quasi-static loading increased by 32% and 28.5%, respectively.

The reviewed studies [12,13,15,17] show for carbon epoxy laminates subjected to 3-point-bending a dependency from loading rate controlled by the initial failure type. All specimens that initially failed due to fiber tension showed no change in maximum force or fracture strain with increasing loading rate. On the contrary, in case of shear, compressive or transversal tension as characteristic failure type the mechanical properties as maximum force and fracture strain increase with increasing loading rate.

In literature, limited information is available to compare the quasi-static and dynamic response of carbon epoxy structures subjected to 3-point-bending. Impact testing is often performed at one specific testing speed to validate the corresponding crash model [18–20] or to obtain the structural component's specific energy absorption (SEA) [21–23], respectively.

Current studies of Belingardi et al. [24] and Fischer et al. [25] investigated the quasi-static and dynamic impact response of composite beams loaded on 3-point-bending. The hybrid specimens [24] were made of a pressed organo sheet stiffened by an injection moulded rib structure. A significant increase in force (ca. 18%) at initial failure was seen between the quasi-static and dynamic (127mm s^{-1}) loading scenario. They concluded for the previously obtained coupons strain rate dependency a continuation on component level. The carbon epoxy hat profiles used by Fischer et al. [25] were made of $[0°/90°/+45°/-45°]_s$ layup and were manufactured in a HP-RTM process. At dynamic testing speed of 3m s^{-1} an increase of initial modulus and maximum load is reported. Using a strain rate-dependent material card obtained form quasi-static and dynamic coupon tests, the experimental and numerical achieved force-displacement curves were in good accordance.

Fagerström et al. [26] used a drop tower to load open carbon epoxy hat profiles at testing speeds ranging from 5 to 10m s^{-1}. Four quasi-static reference tests were performed at 3.6mm s^{-1}. The specimen's layup contained $[90°/0°]_{15s}$, where 0° direction is along the beam's longitudinal direction. Between quasi-static and 5m s^{-1} testing speed an increase of 70% of the maximum force was obtained. Contradictory, is the decrease in maximum force by increasing the testing speed from 5 to 10m s^{-1}. The authors give no explanation for this, but the reported fractography pictures lead to the conclusion of initial failure type by delamination and matrix cracks at the region of the hat profile's shoulder.

The aim of this research is to get a better insight of the characteristics of strain rate evolution from a coupon to a structural component loaded on 3-point-bending. After proving the strain rate evolution for an axial compression load case [2] the current investigation is supposed to investigate a conventional structural crash load case scenario next to axial compression in relation to its strain rate sensitivity. For that purpose quasi-static and dynamic 3-point-bending tests are performed first using rectangular coupon specimens and in a second step carbon epoxy hat profiles. Finally, the experimental data is validated by comparing to numerical simulation results using the developed strain rate-dependent material card from a previous study [2].

2. Materials and specimen preparation

2.1. Materials

The specimens manufactured consist of DT120 (DeltaTech, Altopascio, Italy) epoxy matrix reinforced with high-strength standard-modulus T700S (Toray, Tokyo, Japan) carbon fibers. The unidirectional prepreg tape is 0.5mm thick and has a fiber areal weight of 150 g m^{-2}.

2.2. Rectangular cross section specimens preparation

The 500 x 600mm sized layers of the prepreg material were positioned by hand in 0° direction and were consolidated in the autoclave for 1.5h at 120°C and 6bar pressure. According to that procedure, nine plates were manufactured with different plate thicknesses between 1.49 and 5.52mm. For each plate, nine fiber volume measurements were taken. An average fiber volume content of 54.09% was measured. The cutting of the plates was done with a rotating water-cooled diamond saw. For the 80mm wide support span, the specimens were cut to a length of 100mm and a width of 15mm. For the 60mm wide support distance, the specimens were cut to shorter dimensions, having 80mm in length and 15mm in width. Thus, it was ensured both specimen configurations had a 10mm excess on each side.

2.3. Hat profile cross section specimens preparation

The layers of the prepreg material were manually stacked on a convex hat profiled tool and were consolidated in the autoclave using the same parameters as the coupons from Section 2.2. The hat profile and cover plate were manufactured in one part and process step, obtained by cutting the part in two pieces after curing. The cut was realized at the end of the flange of the hat profile. After trimming the edges of

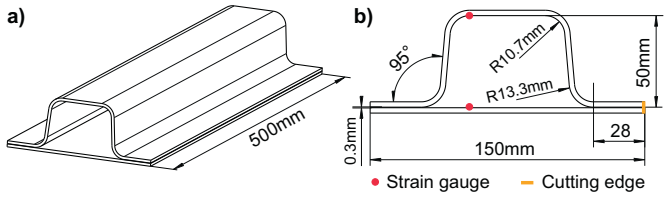

Fig. 1. Schematic view (a) and cross sectional view (b) of the hat profile component with the location of strain gauges and the cutting edge.

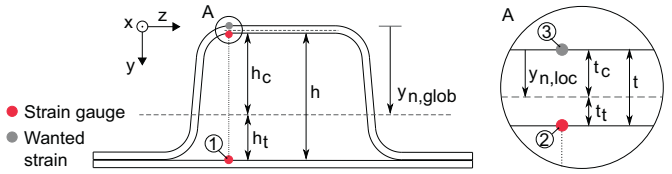

Fig. 2. Strain calculation by using KIRCHHOFF plate theory and the neutral fiber location.

the hat profile, both components were prepared for bonding. Therefore the 28mm wide bonding surface was sandblasted and cleaned with n-Heptan. To bond the cover plates to the flanges of the hat profiles the adhesive type BETAFORCE^{TM} 9050M (DOW®, Midland, USA] was used. To measure strains and strain rates on the inside surface of the hat profiles, two strain gauges were attached before the final bonding of hat profile and cover plate. The specimens were cut with a diamond precision saw DIADISC 5200 (Motronic, Rieden, Germany) to their final dimensions as shown in Fig. 1. Specimens were manufactured with the laminate layups $[0°/90°/+45°/-45°]_{2s}$ and $[90°/0°]_{4s}$.

3. Experimental setup

3.1. Testing equipment

For this work, the purpose was to study the in plane loading behaviour of carbon-epoxy laminates resulting from a out of plane deformation subjected to strain rates varying from the typical quasi-static values (order of magnitude $\times 10^{-5}$ s^{-1} to moderate (up to 100s^{-1}). Therefore, the static and dynamic tests were performed on a Very High Speed VHS 160 (Instron®, Norwood, USA) servo-hydraulic testing machine, using a displacement controlled vertical shaft. Using the same testing machine across the entire considered range of strain rates ensures that the effect of the fixture/machine on the measured results are constant.

The position of the impactor and the specimens deflection were measured by using the digital image correlation (DIC) Software Aramis® (Gesellschaft für optische Messtechnik (GOM), Braunschweig, Germany). Image acquisition was done using two FASTCAM SA-X (Photron, Tokio, Japan) high-speed cameras. The strain in the contact area with the impactor on the hat profile's top surface cannot be measured optically. Therefore the strain is calculated analytically by using the equation (1) and the data from strain gauges applied on the inside surface of the hat profile, as shown in Fig. 2.

$$\varepsilon_3 = \varepsilon_{3,glob} + \varepsilon_{3,loc} = \varepsilon_1 \frac{h_C + t}{h_T} + \left(\varepsilon_2 - \varepsilon_1 \frac{h_C}{h_T}\right)\frac{t_C}{t_T} \quad (1)$$

Whereby ε_1 and ε_2 denote the strains measured with the two applied strain gauges, ε_3 marks the wanted strain on the hat profile's top surface and h_c, h_t, t_c and t_t describe the global and local location of the neutral fiber. These values are based on the KIRCHHOFF plate theory and take different layups including different tensile and compressive properties into account.

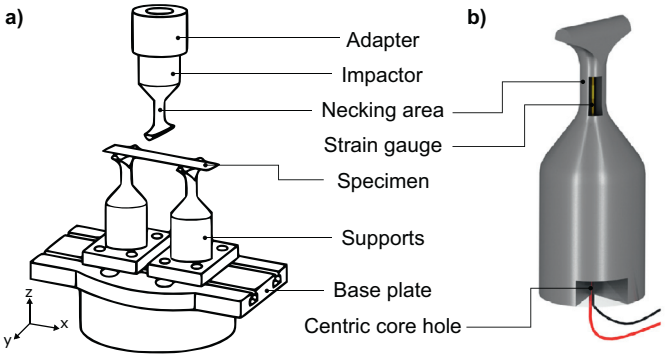

Fig. 3. Self developed component 3-point-bending fixture for coupon specimens (a) and force measuring by using strain gauges (b) [29].

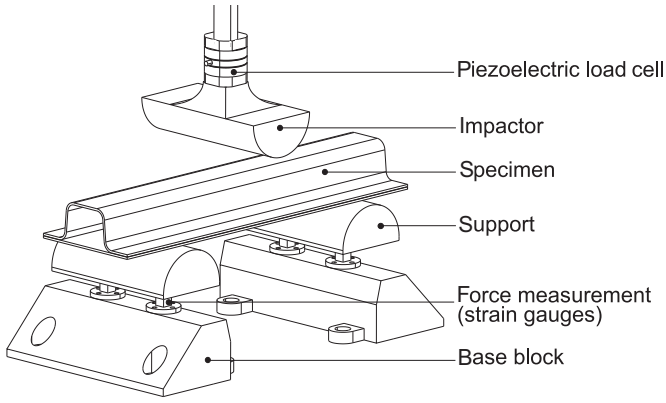

Fig. 4. Self developed component 3-point-bending fixture.

3.2. Laminate 3-point-bending fixture

Based on the standard DIN EN ISO 14125 [27] to determine the flexural properties of fiber reinforced plastics, a new fixture was developed, which is suitable for the conduction of quasi-static (v = 3.3×10^{-5} m s^{-1}) and dynamic (v = 10m s^{-1}) 3-point-bending tests. As shown in Fig. 3 (a) the fixture consists of two supports and one impactor. The impactor and the supports have radii of 5mm and the support distance is variably adjustable. The force measurement is done by strain gauges, which are installed in the bottlenecks of the impactor and the supports through centric core holes, as pictured in Fig. 3 (b). Through the positioning of the strain gauges in the shaft, a direct and unadulterated measurement of the force is reached. To receive reliable absolute force values, the fixture was calibrated with a universal testing machine Z100 (Zwick, Ulm, Germany) according to the standard ISO 7500-1 [28].

3.3. Component 3-point-bending fixture

Because there are no recent standards for the bending tests of components, a new fixture for the conduction of quasi-static and dynamic 3-point-bending tests of components was developed. The new fixture is pictured in Fig. 4.

The impactor and the supports have a radii of 50mm and the support distance is, analogous to the laminate 3-point-bending fixture, variably adjustable. For the force measurement, four strain gauges were applied on each column of the supports and interconnected to a WHEATSTONE full bridge. The arrangement of the strain gauges on the inside and outside of the columns, as well as their horizontal and vertical orientation enables the consideration of the transversal contraction to increase the bridge resolution and the bending-compensated force measurement. Each column was calibrated with a universal testing machine according

Table 1
Load increase of coupons subjected to static (3.08×10^{-5} m s^{-1}) and dynamic (5m s^{-1}) 3-point-bending with the corresponding coefficient of determination R^2 for each configuration.

Support Span [mm]	Beam Thickness [mm]	Max. Load at 3.08×10^{-5} m s^{-1} [kN]	CoD R^2 [−]	Max. Load at 5m s^{-1} [kN]	CoD R^2 [−]	Load Increase from 3.08×10^{-5} to 5m s^{-1} [kN]	Load Increase from 3.08×10^{-5} to 5m s^{-1} [%]
80	1.50	414.56 ± 15.37	0.942	482.77 ± 68.21	0.733	68.21	16%
80	1.95	724.01 ± 46.93	0.981	765.47 ± 126.61	0.786	41.46	6%
80	2.55	1050.50 ± 78.81	0.977	1409.40 ± 89.50	0.837	358.90	34%
80	3.00	1307.80 ± 75.27	0.991	1764.40 ± 113.57	0.839	456.60	35%
80	3.45	1588.30 ± 29.61	0.993	2305.50 ± 95.17	0.868	717.20	45%
80	4.05	1995.50 ± 31.51	0.994	2947.80 ± 67.07	0.898	952.30	48%
80	4.50	2298.70 ± 48.30	0.995	3382.40 ± 21.73	0.906	1083.70	47%
80	4.95	2624.70 ± 46.29	0.996	4178.30 ± 163.50	0.930	1553.60	59%
80	5.55	3159.90 ± 266.10	0.996	4660.70 ± 221.27	0.927	1500.80	47%
60	1.50	622.26 ± 37.14	0.970	672.34 ± 27.65	0.866	50.08	8%
60	1.95	951.98 ± 30.39	0.981	1184.30 ± 43.97	0.890	232.32	24%
60	2.55	1400.10 ± 54.06	0.990	1845.70 ± 82.85	0.949	445.60	32%
60	3.00	1793.60 ± 113.08	0.990	2322.80 ± 76.40	0.948	529.20	30%
60	3.45	2177.50 ± 68.33	0.994	2849.70 ± 95.36	0.962	672.20	31%
60	4.05	2686.90 ± 10.45	0.995	3839.20 ± 133.74	0.972	1152.30	43%
60	4.50	3237.80 ± 72.35	0.994	4435.70 ± 79.346	0.969	1197.90	37%
60	4.95	3663.30 ± 33.89	0.995	5279.90 ± 408.77	0.973	1616.60	44%
60	5.55	4662.90 ± 75.36	0.993	6934.70 ± 642.67	0.938	2271.80	49%

to the standard ISO 7500-1 [28]. In addition, the force is measured by a piezoelectric force sensor installed above the impactor. The impactors mass and the high accelerations result in inertia forces, which distort the force signal. For the correction of the force signal, impactors accelerations are first determined using DIC, then multiplied by the impactors mass, and last subtracted from the measured force signal. With this method, the measured force signals of the support columns and the impactor correlate. Because of restrictions of signal processing due to the use of strain gauges on the specimen, the reported results in this paper are the corrected force signal of the piezoelectric force sensor.

4. Experimental results

4.1. Rectangular cross section specimens

The unidirectional specimens with the nine different thicknesses were tested with two different support distances (60mm and 80mm) and with different impactor velocities between 3.3×10^{-5} m s^{-1} and 10m s^{-1}. For every parameter combination 3 replicates were performed. The mechanical response of the UD laminate subjected to 3-point-bending are summarized in Tab. 1.

The aim of studying this broad variety of thicknesses, two support spans and different testing speeds was to determine the reliability of measured maximum force and maximum midpoint displacement. The results show a significant influence of testing speed on the vibrations of the force signal, as shown in Fig. 5. So, based on the analysis of the test data comparing the coefficient of determination R^2 (CoD) of linear fits to every single force displacement curve, it was concluded that, for the unidirectional carbon/epoxy composite tested, the best configuration would be the one that has a support span of 60mm and a thickness between 4 and 4.5mm. These configurations were the ones that gave low standard deviation in the test results and minimised the specimen detachment from the impactor. An explanation is the increasing beam stiffness with increasing specimen thickness and decreasing support span, which leads to less vibrations during the test and more reliable results. Nevertheless, in the previous sections all available data is presented.

For laminate thicknesses < 3mm at 80mm support distance strong vibrations and no increase in maximum force have been observed. Whereas for laminate thicknesses ≤ 3mm an increase of the maximum force and the maximum deflection with increasing testing velocity has been determined as shown in Fig. 6. In comparison with the quasi-static results, the results at the lowest dynamic impactor velocity showed an increase of over 20% for the maximum force and the maximum deflec-

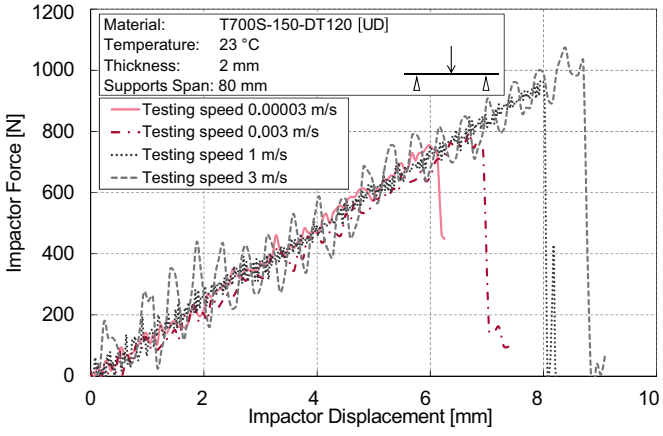

Fig. 5. Exemplary force displacement curves of coupons loaded on 3-point-bending with support span of 80mm with the resulting increase of vibrations in the force signal with increasing testing speed.

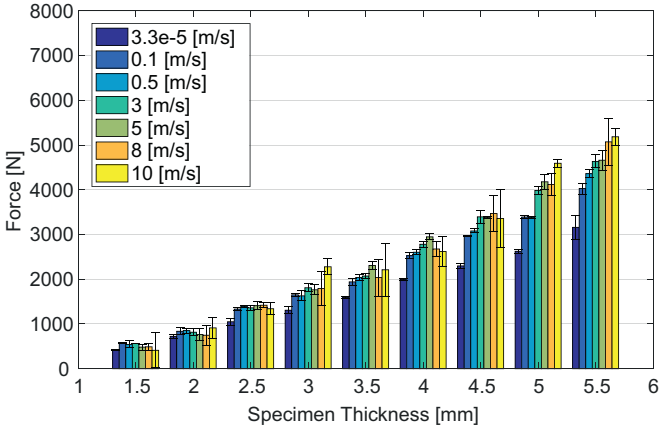

Fig. 6. Maximum force of coupons with different thicknesses loaded on 3-point-bending with support span of 80mm at various strain rates.

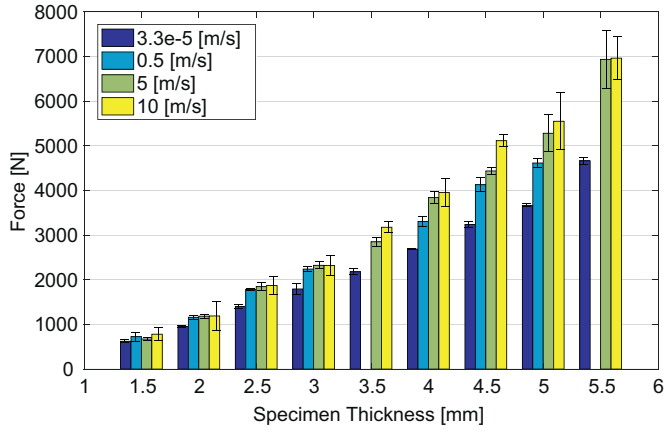

Fig. 7. Maximum force of coupons with different thicknesses loaded on 3-point-bending with support span of 60mm at various strain rates.

tion. For the highest impactor velocity, the maximum force increased up to 74% compared to the quasi-static result. For laminate thicknesses ≥ 3.5mm, an increase of the maximum deflection of 100% up to 120% was determined, whereas the maximum deflection of the thinner laminates increased less with higher impactor velocities (40% up to 63%).

The specimens tested with the 60mm support distance also showed a significant increase of the maximum force (up to 58%) and the maximum deflection (up to 95%) with higher impactor velocities as shown in Fig. 7. Compared to the tests with 80mm support distance, a lower scatter was determined. An explanation for that is the reduced amount of vibrations during the test procedure.

In every experiment, fiber compressive failure (kinking) as initial failure mechanism was observed. Initial failure on the compressive side of the specimen was also reported by Wiegand [15]. For the clarification of the reproducible failure mechanism, a low flexural stiffness configuration with a 80mm support distance, a 3.5mm thick specimen and a testing velocity of v = 5m s^{-1} is shown in Fig. 8 (a). The high flexural stiffness configuration with the same support distance and testing velocity, but with a 5mm thick specimen is pictured in Fig. 8 (b).

The mentioned compressive failure type was expected due to the known lower compressive laminate strength compared to tensile strength, as already reported in a previous study [2]. In addition, the axial and flexural loaded laminates show both an increase of the investigated in plane mechanical properties with increasing strain rate. Triggered by the compressive failure the increasing maximum force and maximum deflection from the 3-point-bending scenario follow the trend of increasing laminate properties loaded on axial compression.

4.2. Hat profile cross section specimens

The 3-point-bending tests were performed using three different impactor velocities from 6mm min^{-1} to 1m s^{-1}, two different laminate layups (biaxial $[90°/0°]_{4s}$) and quasi-isotropic $[0°/90°/+45°/-45°]_{2s}$) and a support distance of 260mm. To ensure the reliability of the measured data five replicates for each configuration were conducted. Fig. 9 exemplary shows the failure progress of a $[90°/0°]_{4s}$ hat profile specimen loaded on 3-point-bending using a support span of 260mm at a testing speed of 1m s^{-1} in 6 increments of impactor displacement. The failure type and progression in the investigated area of velocity is independent from the loading rate. At 10mm impactor displacement a local intrusion of the specimen is causing a interlaminar failure due to high transverse shear stresses, as shown in Fig. 10. After this first failure a further intrusion of the impactor in the hat profile's web is observed, and after 48mm the maximum loading capacity of the specimen is reached. With progressing impactor displacement the hat profile's neutral axis shift constantly down what is causing at ca. 30mm impactor displacement fiber compression failure in the flanges and the cover plate. The ultimate failure occurs at ca. 48mm impactor displacement (Fig. 9).

For the experiments of the hat profiles with the biaxial laminate layup at the highest impactor velocity, there was a significant increase for the force at first failure compared to the quasi-static result. Fig. 10 depicts the computed tomography (CT) scan of the hat profile shoulder after the first failure. The scan shows that the first failure is initiated by delamination and the occurrence of matrix cracks at the hat profile

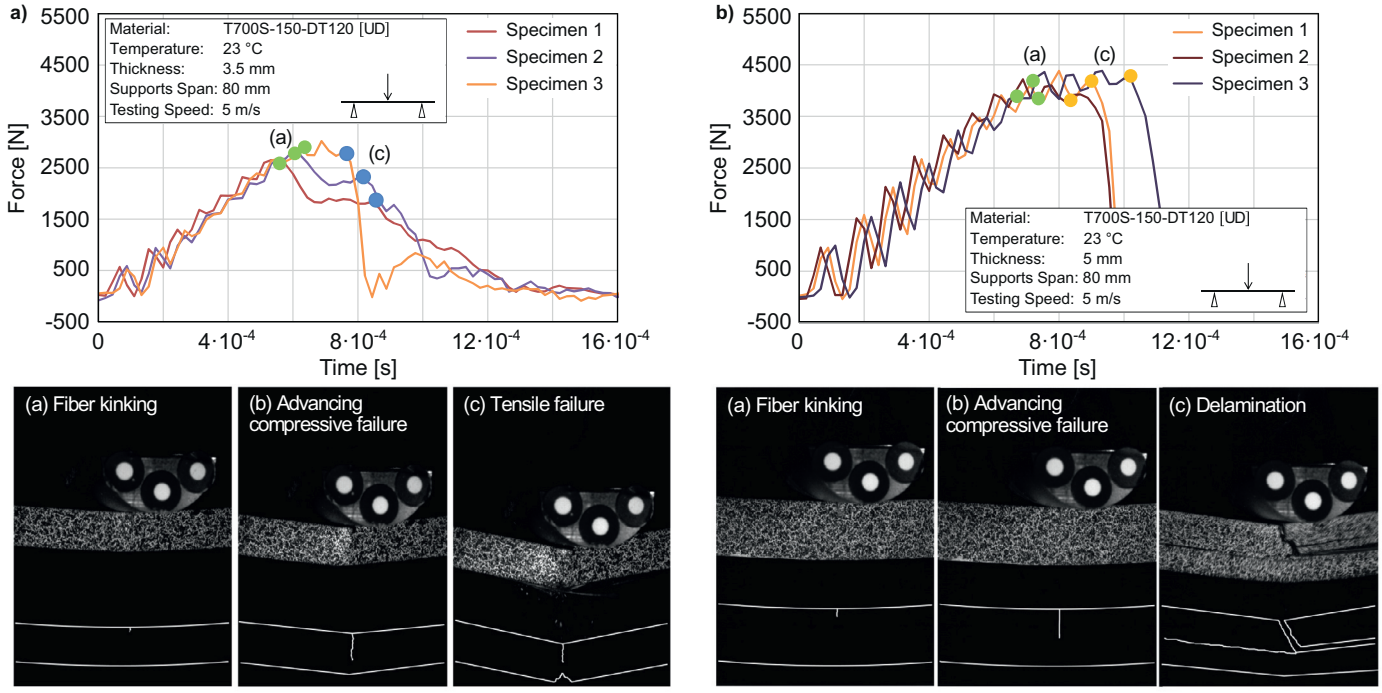

Fig. 8. Failure mechanism of 3.5mm (a) and 5mm (b) thick specimens. Support span of 80mm at a testing velocity of 5m s^{-1}.

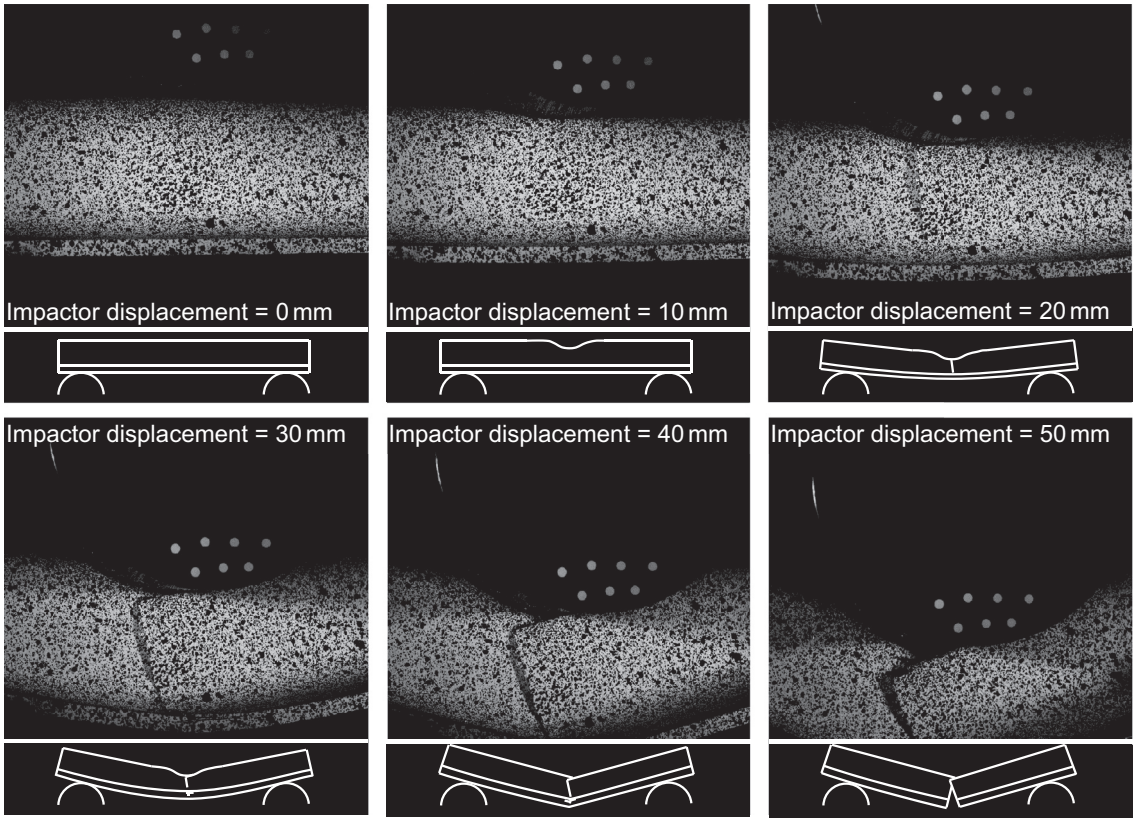

Fig. 9. Typical failure progress of a $[90°/0°]_{4s}$ hat profile specimen loaded on 3-point-bending in 6 increments of deflection using a support span of 260mm at a testing speed of 1m $s^{-}1$.

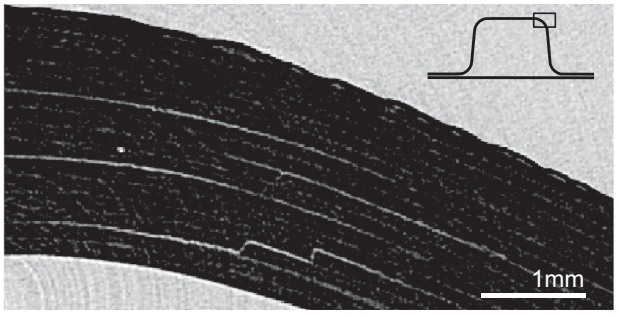

Fig. 10. CT-scan showing the delaminations in radius between top surface and web of the hat profile.

Table 2
Experimental results of the hat profile components with $[0°/90°]_{4s}$ layup at three different testing speeds.

	Impactor Velocity [m/s]	Mean Value ± Standard Deviation	Mean related to quasi-static Value [%]
Load at first Failure	10^{-4}	6.12 ± 0.21 kN	-
	10^{-2}	6.65 ± 0.16 kN	+8.7
	1	6.88 ± 0.27 kN	+12.4
Maximum Load	10^{-4}	15.1 ± 0.7 kN	-
	10^{-2}	14.8 ± 0.8 kN	-1.9
	1	15.9 ± 0.4 kN	+5.5
Initial Stiffness	10^{-4}	2.40 ± 0.16 kN/mm	-
	10^{-2}	2.53 ± 0.13 kN/mm	+5.4
	1	2.88 ± 0.36 kN/mm	+19.8
Energy Absorption	10^{-4}	670 ± 64 J	-
	10^{-2}	706 ± 35 J	+5.4
	1	692 ± 55 J	+3.3

shoulder. Consequently the increase of strength with higher testing velocities is a result of the strain rate-dependent shear properties of the matrix, which brittles with increasing testing velocities. Fiber compressive failure on the top surface of the hat profile as initial failure can be ruled out because the measured compression at the failure moment was significantly below the fracture strain.

The initial stiffness shows in the respective testing velocity range a slight increase of 19.8% with no statistical significance. While the maximum force and the specific energy absorption show no increase at all with increasing testing speed. This results are in accordance with previous investigations of the strain rate dependency on the crushing properties of CFRP [30–32]. The respective results are summarized in Table 2.

Nevertheless, for hat profiles containing the $[0°/90°/45°/-45°]_{2s}$ layup the force at initial failure increased significantly by 18.8%. A CT analysis of a specimen loaded quasi-statically just to its first failure shows a delamination in the hat profile radius connecting the horizontal top surface and the vertical web (shoulder), as shown in Fig. 10. In accordance with the biaxial $[90°/0°]_{4s}$ specimens, the strain rate dependency results from the strength increase of the matrix' shear properties with increasing strain rate. For the initial stiffness an increase of 41.1% was determined. However the significance of this value is low because of the high scatter. One possible explanation for the stiffness increase is the embrittlement of the matrix in the failure critical areas of the hat profile shoulders. The maximum force increased by 6.3% but did not show a general trend, which would indicate a strain rate dependency of this value. For the energy absorption there was not a significant change with increasing testing velocities. The results for the quasi-isotropic layup are summarized in Table 3, while an overall comparison of both layups is depicted in Fig 11.

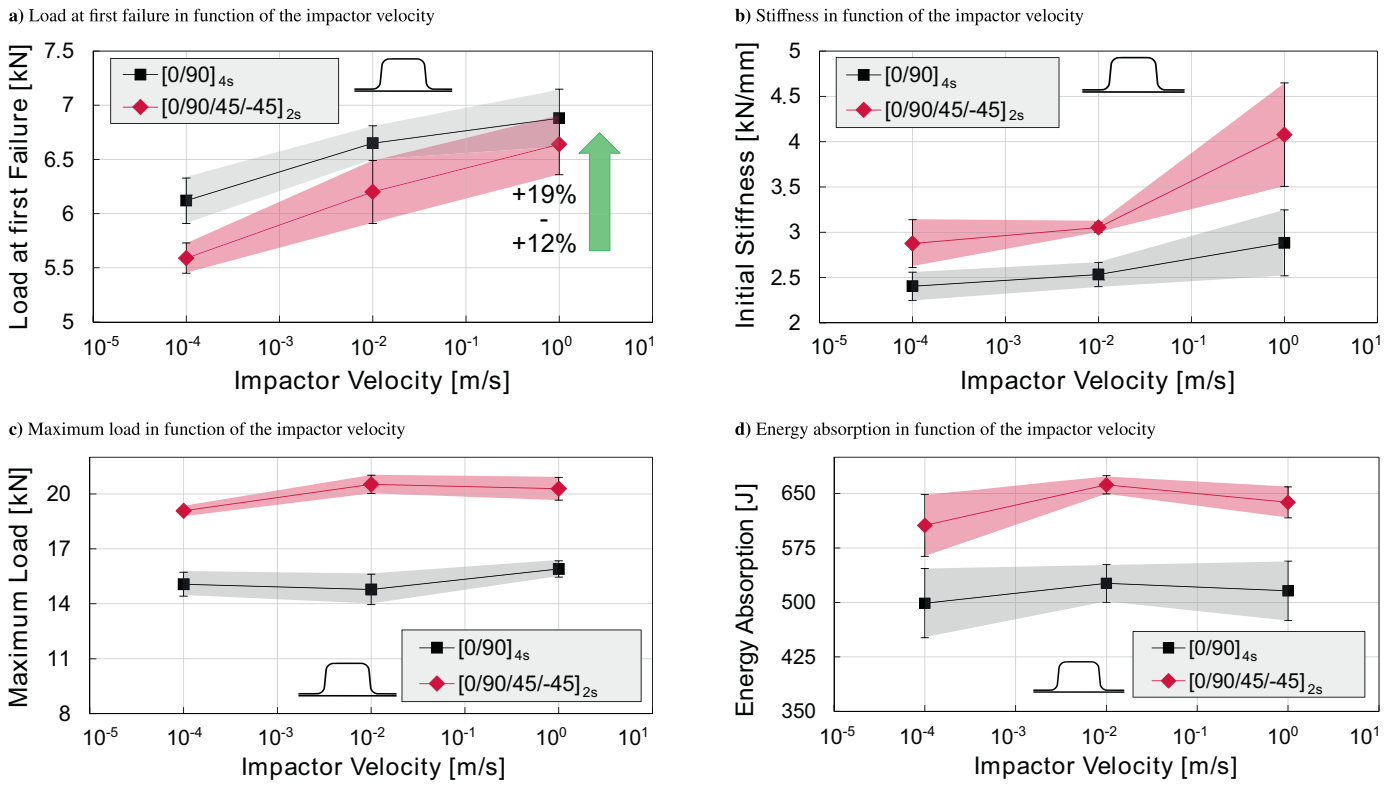

Fig. 11. Experimental results for load at first failure, maximum load, initial stiffness and energyabsorption (up to 50 mm impactor displacement) of hat profile specimens loaded with different impactor velocities.

Table 3
Experimental results of the hat profile component with $[0°/90°/45°/-45°]_{2s}$ layup at three different testing speeds.

	Impactor Velocity [m/s]	Mean Value ± Standard Deviation	Mean related to quasi-static Value [%]
Load at first Failure	10^{-4}	5.59 ± 0.14 kN	-
	10^{-2}	6.20 ± 0.29 kN	+10.9
	1	6.64 ± 0.28 kN	+18.8
Maximum Load	10^{-4}	19.1 ± 0.2 kN	-
	10^{-2}	20.5 ± 0.5 kN	+7.5
	1	20.3 ± 0.6 kN	+6.3
Initial Stiffness	10^{-4}	2.88 ± 0.26 kN/mm	-
	10^{-2}	3.05 ± 0.06 kN/mm	+5.9
	1	4.07 ± 0.57 kN/mm	+41.1
Energy Absorption	10^{-4}	606 ± 42 J	-
	10^{-2}	661 ± 12 J	+9.1
	1	638 ± 21 J	+5.3

5. Numerical model

The simulations were carried out using the commercially available explicit Finite Element software Pam-Crash from ESI. Since the automotive industry requires computation efficiency as well as practical models for pre- and postprocessing, a ply based concept is used. The one part shell elements have as many through thickness integration points as plies defined for the laminate. The ply mechanics are based on a continuum damage approach proposed by Ladeveze and Le Dantec [33]. The strain rate-dependent model is based on the work of Rozycki [34] and it consists of using viscosity functions to describe the variation of the ply properties with the strain rate. The implementation of the strain rate dependent properties of the material used in this work, is carried over from a previous work [2].

6. Numerical simulation results and comparison

A simulation model that depicts the experimental crash tests performed with a hat profile cross section structural component was developed using the previously described numerical model. The simulation impact velocity was chosen analogous to the experimentally obtained one.

For all the examined configurations the initial stiffness is in good accordance with the experimental determined values, as the comparison of the force-displacement curves shows, pictured in Fig. 12. The simulation model overestimates the force at first failure by an amount between 14% and 32%. The explanation is the difference in failure mechanisms that lead to initial failure. In the experiment, the initial failure mechanisms are delamination and matrix cracking. The simulation model however cannot describe delamination, which is why the force increases steadily until fiber-compression failure occurs at the hat profile top surface. The increase of strength at 1m s^{-1} impactor velocity compared to the quasi-static value only amounts 1.9% in the simulation. However, the increase in the simulation is based on the strain-rate-dependent compression properties and is, for that reason, not comparable with the experimental results, where the strain-rate dependency of the shear properties are of primary importance. For the hat profiles with biaxial laminate layup, the maximum force and the nearly constant force level are underestimated by the simulation. The usage of a nominal laminate thickness of 2.4mm in the simulation, instead of an actual average laminate thickness of 2.49mm is one possible explanation for the deviation. For the quasi-isotropic laminate layup, the simulation underestimates the maximum force by approximately 30%. For the high deviation of the experiments with this laminate layup there is a second possible explanation besides the difference in the used laminate thickness. The maximum force is reached before the webs collapse because of the global bending. In the used material card, the fracture strain of the 0°-plies refers to values, which where determined by testing an UD

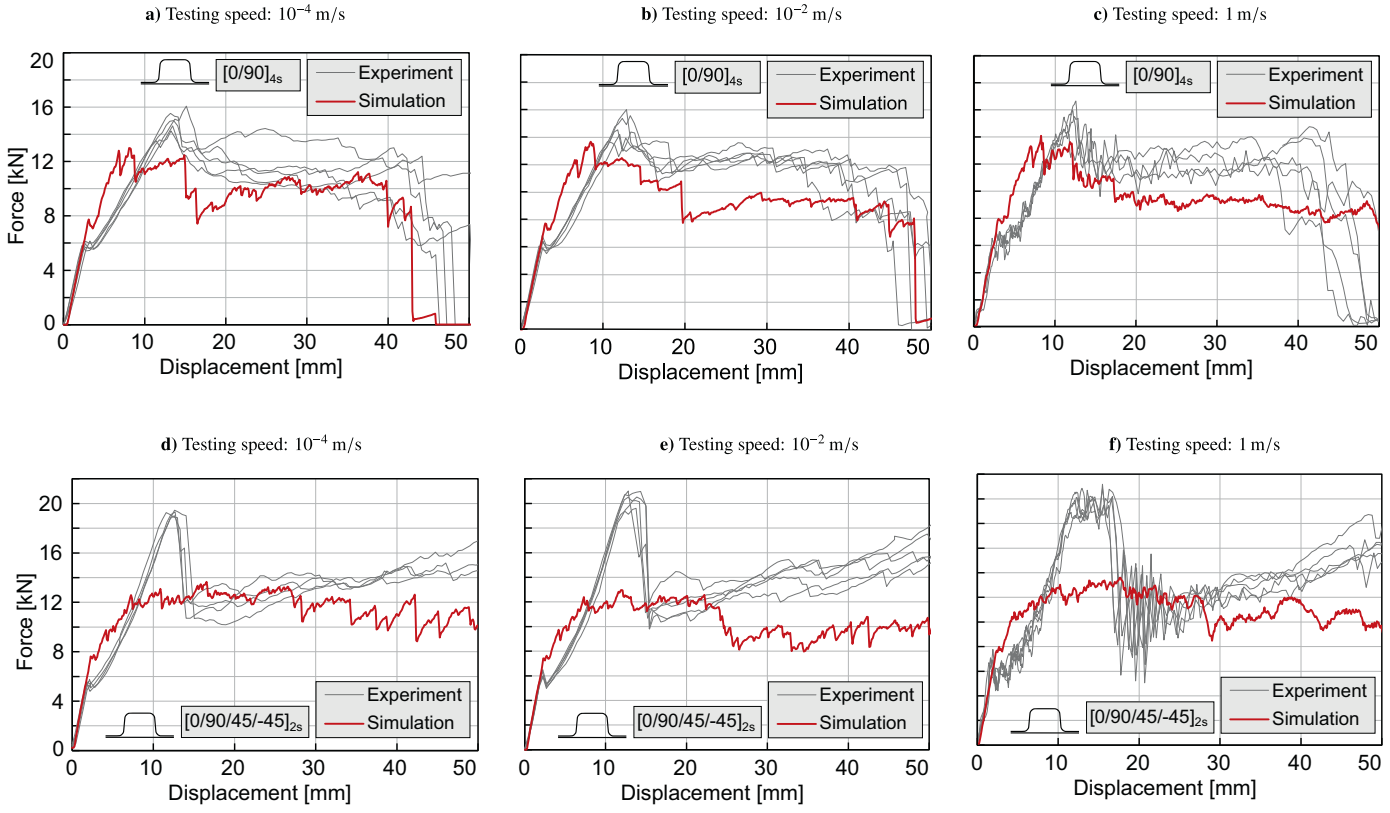

Fig. 12. Experimental and simulation force vs. displacement curves for hat profile specimens.

laminate. Hence, the presence of off axis plies has no impact on the fracture strain in the simulation. In the experiment the 0°-plies are supported by the off axis plies against buckling and therefore reach higher fracture strains. The higher fracture strains of the 0°-plies lead to higher maximum forces before the webs of the hat profile collapse.

7. Conclusions

The coupon specimens composed of T700 DT120 prepreg with unidirectional layup manufactured in different thicknesses were loaded on 3-point-bending with respect to different loading rates. The results confirm the well known longitudinal compressive strain rate-dependency [2] for a 3-point-bending loading scenario. With increasing impactor speed, the maximum load at failure and the deflection increased up to 74% and 120%, respectively. Furthermore, all tested specimens showed as result of fiber kinking a compressive failure at the top side of the specimen as initial failure mode. Hence, the increasing properties with increasing loading rate under 3-point-bending are correlated to the laminate longitudinal compressive properties, as shown in previous work [2].

On a second level of scale, a hat profile, more comparable to a structural component, composed of the identical material was loaded on 3-point-bending at 3 different testing velocities. The hat profile contained a biaxial $[90°/0°]_{4s}$) and quasi-isotropic $[0°/90°/+45°/-45°]_{2s}$ layup and resulted in a load increase of up to 18.8% at dynamic rates at first failure with respect to the quasi-static loading rate. As initial failure type delaminations in the hat profile's shoulder were detected by a CT analysis performed on a specimen loaded quasi-statically until its first failure. The detailed investigation of this effect using the numerical model led to the conclusion of transverse shear strength reaching its limit at the moment of first failure of the specimen. Thus, the increase in maximum force at first failure with increasing strain rate is associated to the strain rate-dependent change in shear properties of the matrix material.

The results of the numerical simulation based on shell elements made obvious that the missing ability to consider delaminations by this element type is the restrictive parameter in prediction accuracy of the hat profiles first failure as response to 3-point-bending. Consequently, in future work hat profiles loaded on 3-point-bending can just be accurately predicted by using e.g. cohesive zone interface elements or tiebreak contacts in between a multi shell stack, as already presented by [35,36].

The comparison of the occurring failure types in combination with the numerical simulation results between the coupon and hat profile leads to following conclusions: i) the coupon reaches its maximum load capacity by reaching the compressive strength of the material and thus shows a much higher increase with respect to strain rate. ii) the hat profile is limited in loading capacity due to local failure triggered by delamination in its shoulders. iii) the used hat profile geometry is limited to its ability to validate structures which are in direct contact of a barrier (e.g. rocker in a side pole crash scenario). iv) the differences in failure type made a comparison impossible in terms of strain rate dependency of a coupon compared to a structural component subjected to 3-point-bending.

Declaration of interests

The authors declare that they have no known competing financial interests or personal relationships that could have appeared to influence the work reported in this paper.

Acknowledgements

The authors gratefully thank the German Federal Ministry of Education and Research for the funding of the project SMiLE "System-integrated multi-material lightweight design for e-mobility" (03X3041).

References

[1] T. Schmack, T. Jansen, T. Filipe, M.H. Kothmann, F. Walther, Development of a new standard for dynamic properties characterisation of cfrp, in: J. Remmers, A. Turon (Eds.), Proceedings of the sixth ECCOMAS Thematic Conference on the Mechanical Response of Composites, Eindhoven University of Technology, 2017, pp. 271–283.

[2] T. Schmack, T. Filipe, G. Deinzer, C. Kassapoglou, F. Walther, Experimental and numerical investigation of the strain rate-dependent compression behaviour of a carbon-epoxy structure, Compos. Struct. 189 (2018) 256–262, doi:10.1016/j.compstruct.2017.11.025.

[3] R.M. Guedes, M. de Moura, F.J. Ferreira, Failure analysis of quasi-isotropic cfrp laminates under high strain rate compression loading, Compos. Struct. 84 (4) (2008) 362–368, doi:10.1016/j.compstruct.2007.10.001.

[4] R.O. Ochola, K. Marcus, G.N. Nurick, T. Franz, Mechanical behaviour of glass and carbon fibre reinforced composites at varying strain rates, Compos. Struct. 63 (3–4) (2004) 455–467, doi:10.1016/S0263-8223(03)00194-6.

[5] M. Hosur, J. Alexander, U. Vaidya, S. Jeelani, High strain rate compression response of carbon/epoxy laminate composites, Compos. Struct. 52 (3–4) (2001) 405–417, doi:10.1016/S0263-8223(01)00031-9.

[6] H.M. Hsiao, I.M. Daniel, Strain rate behavior of composite materials, Composites Part B: Engineering 29 (5) (1998) 521–533, doi:10.1016/S1359-8368(98)00008-0.

[7] H. Koerber, P.P. Camanho, High strain rate characterisation of unidirectional carbon–epoxy im7-8552 in longitudinal compression, Composites Part A: Applied Science and Manufacturing 42 (5) (2011) 462–470, doi:10.1016/j.compositesa.2011.01.002.

[8] Q. Bing, C. Sun, Modeling and testing strain rate-dependent compressive strength of carbon/epoxy composites, Compos. Sci. Technol. 65 (15–16) (2005) 2481–2491, doi:10.1016/j.compscitech.2005.06.012.

[9] T. Schmack, D. Huelsbusch, R. Righi, J. Rausch, D. Roquette, G. Deinzer, F. Walther, Influence of load application and fixtures on characteristic values at short-time dynamic compression testing of carbon fiber-epoxy composites, in: European Society for Composite Materials (Ed.), Proceedings of the ECCM17 - 17th European Conference on Composite Materials, European Society for Composite Materials (ESCM), 2016, pp. 1–2, doi:10.1016/B978-0-12-802121-7.01601-0.

[10] N. Taniguchi, T. Nishiwaki, H. Kawada, Tensile strength of unidirectional cfrp laminate under high strain rate, Adv. Compos. Mater 16 (2) (2007) 167–180, doi:10.1163/156855107780918937.

[11] I.M. Daniel, R.H. LaBedz, T. Liber, New method for testing composites at very high strain rates, Exp. Mech. (1980) 71–77.

[12] J.M. Lifshitz, F. Gov, M. Gandelsman, Instrumented low-velocity impact of cfrp beams, Int. J. Impact Eng. 16 (2) (1995) 201–215, doi:10.1016/0734-743X(94)00048-2.

[13] S. Sánchez-Sáez, E. Barbero, C. Navarro, Analysis of the dynamic flexural behaviour of composite beams at low temperature, Compos. Sci. Technol. 67 (11–12) (2007) 2616–2632, doi:10.1016/j.compscitech.2006.12.002.

[14] J. Harding, L.M. Welsh, A tensile testing technique for fibre-reinforced composites at impact rates of strain, Material Science 1983 (1983) 1810–1826.

[15] J. Wiegand, Constitutive modelling of composite materials under impact loading, University of Oxford, Oxford, 2008 Phd.

[16] S.R. Hallett, Three-point beam impact tests on t300/914 carbon-fibre composites, Compos. Sci. Technol. 60 (1) (2000) 115–124, doi:10.1016/S0266-3538(99)00099-8.

[17] A.P. Carpentier, Advanced Materials Characterization Based on Full Field Deformation Measurements, The University of Texas at Arlington, Arlington, Texas, 2013 Phd.

[18] D. Moncayo, F. Köster, P.P. Camanho, D. Coutellier, S. Hartmann, Modelling laminate failure in composite materials for automotive applications, FEA Information Engineering Journal 5 (06) (2016).

[19] F. Köster, F. Henning, D. Moncayo, Approaches for an advanced modeling technique for component design and prediction of the laminate failure in thick multilayered composites, FEA Engineering Journal 5 (06) (2016) 1–44.

[20] R. Pasupuleti, Validation material models design and analysis composite front bumper crush can system, in: Automotive Composites Conference & Exhibition, Society of Plastic Engineers, 2016, pp. 1–21.

[21] D. Emerson, D. Almond, N. Reynolds, D.J. Hughes, M. Pharaoh, Williams. Geraint J., Energy absorbtion characteristics of automotive-type beam structures in high-speed crush testing, in: Proceedings of Automotive Composites Conference & Exhibition, 2013, pp. 1–18.

[22] L. Berger, O. Faruque, Validation of material models for crash simulation of automotive carbon fiber composite structures (vmm), 2016.

[23] E. Irving, E. Phil, C. Soutis, Polymer composites in the aerospace industry, Woodhead Publishing series in composites science and engineering, Elsevier, 2014, 2014.

[24] G. Belingardi, H. Mehdipour, E. Mangino, B. Martorana, Progressive damage analysis of a rate-dependent hybrid composite beam, Compos. Struct. 154 (2016) 433–442, doi:10.1016/j.compstruct.2016.07.055.

[25] S. Fischer, A material model for fe-simulation of ud composites, Appl. Compos. Mater. 23 (2) (2016) 197–217, doi:10.1007/s10443-015-9456-1.

[26] M. Fagerström, R. Larsson, R. Olsson, J. Främby, G. Peterson, J. Jergeus, F. Stig, D. Lundgren, T. Andersson, T. Bru, Modelling crash behaviour in future lightweight composite vehicles - step 1: (final report), 2016.

[27] DIN EN ISO 14125, Fibre-reinforced plastic composites - determination of flexural properties: Determination of flexural properties, 1998.

[28] DIN EN ISO 7500-1, Metallic materials - calibration and verification of static uniaxial testing machines - part 1: Tension/compression testing machines - calibration and verification of the force-measuring system, 1999.

[29] T. Schmack, R. Righi, D. Huelsbusch, J. Rausch, D. Roquette, G. Deinzer, M.H. Kothmann, C. Kassapoglou, F. Walther, A newly-developed fixture and testing method for strain rate-dependent flexural properties determination of carbon/epoxy laminates, in: Chinese Society for Composite Materials (Ed.), Proceedings of 21st International Conference on Composite Materials, 2017, pp. 1–12.

[30] G.l. Farley, Energy absorption of composite materials, J. Compos. Mater. 17 (3) (1983) 267–279, doi:10.1177/002199838301700307.

[31] P.H. Thornton, J.J. Harwood, P. Beardmore, Fiber-reinforced plastic composites for energy absorption purposes, Compos. Sci. Technol. 24 (1985) 275–298.

[32] L.N. Chiu, B.G. Falzon, D. Ruan, S. Xu, R.S. Thomson, B. Chen, W. Yan, Crush responses of composite cylinder under quasi-static and dynamic loading, Compos. Struct. 131 (2015) 90–98, doi:10.1016/j.compstruct.2015.04.057.

[33] P. Ladeveze, E. Ledantec, Damage modelling of the elementary ply for laminated composites, Compos. Sci. Technol. 43 (1992) 257–267.

[34] M.P. Rozycki, Contribution au developpement de lois de comportement pour materiaux composites soumis a l'impact, Université de Valenciennes and du Hainaut Cambrésis, 2000 Phd thesis.

[35] B. Stier, J.-W. Simon, S. Reese, Finite element analysis of layered fiber composite structures accounting for the material's microstructure and delamination, Appl. Compos. Mater. 22 (2) (2015) 171–187.

[36] F. Dogan, H. Hadavinia, T. Donchev, P. Bhonge, Delamination of impacted composite structures by cohesive zone interface elements and tiebreak contact, Open Engineering 2 (4) (2012) 612–626.